

COMPONENT SEPARATION FOR FUTURE CMB B-MODE SATELLITES

M. REMAZEILLES

*Jodrell Bank Centre for Astrophysics, School of Physics and Astronomy, Alan Turing Building,
The University of Manchester, Oxford Road, Manchester, M13 9PL, U.K.*



Next-generation CMB satellite concepts (*LiteBIRD*, *CORE*, *PIXIE*, *PICO*) are being proposed to detect the primordial CMB B-mode polarization at large angular scales in the sky for tensor-to-scalar ratio values of $r \lesssim 10^{-3}$. Yet undetected, primordial CMB B-modes will provide the unique signature of the primordial gravitational waves of quantum origin predicted by inflation. We present recent forecasts on the detection of the primordial CMB B-modes in the presence of astrophysical foregrounds and gravitational lensing effects, in the context of the proposed CMB space mission *CORE*. We also discuss the problem of foregrounds and component separation for the search for primordial B-modes, and highlight specific challenges in this context: frequency range, spectral degeneracies, foreground modelling, spectral averaging effects.

1 Introduction

The search for the primordial B-mode polarization of the cosmic microwave background (CMB) radiation at large angular scales in the sky is one of the most exciting challenge of modern cosmology, because such a signal would be the direct signature of the primordial gravitational waves predicted by inflation¹. The amplitude of the primordial B-mode signal, termed as tensor-to-scalar ratio, r , will determine the energy scale of inflation, $E_{\text{inf}} \simeq (r/0.008)^{\frac{1}{4}} 10^{16}$ GeV. CMB satellite concepts (*LiteBIRD*², *CORE*³, *PIXIE*⁴, *PICO*⁵) are being proposed to detect large-scale CMB B-modes at $r \lesssim 10^{-3}$. This is a real challenge because the signal is extremely faint ($\lesssim 50$ nK r.m.s. fluctuations in the sky) and obscured by very bright polarized Galactic foreground emissions by many orders of magnitude. In addition, gravitational lensing effects by large-scale structures transform CMB E-modes into noise-like B-modes, while spurious B-modes are created by instrumental systematic effects. In this context, component separation methods are critical to subtract the foregrounds and extract the CMB B-mode signal, since the residual foreground contamination will set the ultimate uncertainty limit with which r can be measured.

In this article, we report on recent B-mode detection forecasts with the CMB satellite concept *CORE*⁶, and briefly discuss about the problem of foregrounds and component separation for B-modes, by highlighting subtle issues that arise in this context.

2 B-mode component separation forecasts for *CORE*

The proposed space mission *CORE*³ is designed to observe the full sky with high sensitivity through 19 frequency bands, ranging from 60 to 600 GHz. We report on the results⁶ of component separation and primordial CMB B-mode reconstruction, based on *CORE* sky simulations.

2.1 Sky simulations

Using the PSM (Planck Sky Model) software⁷, we have simulated full-sky polarization maps for the 19 frequency bands (60 to 600 GHz) of *CORE*. Our simulated sky maps⁶ include: CMB E- and B-mode polarization, with an optical depth to reionization $\tau = 0.055$ and a tensor-to-scalar ratio ranging from $r = 10^{-3}$ to 10^{-2} ; lensing E- and B-modes; Galactic and extra-galactic foreground polarization. Galactic foregrounds consist of thermal dust emission, based on the *Planck* GNILC dust template⁸ at 353 GHz, with average polarization fraction of 5-10% over the sky; polarized Galactic synchrotron emission, as observed by *WMAP* at 23 GHz⁹; and Galactic anomalous microwave emission (AME) with 1% polarization fraction. Extra-galactic foregrounds include compact radio and infrared sources with respectively 3%-5% and 1% mean polarization fractions. The dust map is interpolated across the *CORE* frequency bands through a modified blackbody (MBB) emission law having variable spectral index and temperature over the sky, with mean values $\langle\beta_d\rangle = 1.6$ and $\langle T_d\rangle = 19.4$ K, as measured by *Planck*⁸. The synchrotron map is extrapolated across frequencies through a power-law with an average spectral index of $\langle\beta_s\rangle = -3$ varying over the sky⁹. The emission law for extrapolating the AME component is modelled by assuming a Cold Neutral Medium¹⁰. Compact source templates are extrapolated across *CORE* frequencies by assuming random steep or flat power-laws for radio sources, and both modified blackbodies and power-laws for infrared sources. The component maps at each frequency are coadded, convolved by a Gaussian beam using the *CORE* FWHM values, and instrumental white noise is added to each frequency map using the sensitivities quoted by *CORE*³.

2.2 Component separation methods

We have applied four independent component separation algorithms⁶ to the *CORE* sky simulations to perform foreground removal, reconstruction of the CMB B-mode power spectrum, and estimation of the tensor-to-scalar ratio: COMMANDER¹¹, a Bayesian parametric method for a multi-component pixel-by-pixel spectral fit using MCMC Gibbs sampling; SMICA¹¹, a blind method for a power-spectra fit in harmonic space; NILC¹¹, a blind method for minimum-variance internal linear combination in wavelet space; and xFORECAST¹², an alternative parametric fitting approach in pixel space. The first three algorithms have already a strong heritage from real *Planck* data analysis¹¹. Parametric methods are only limited by the accuracy with which the foregrounds are modelled in the fit, while blind methods do not rely on any assumptions about the foregrounds but are limited by the overall variance of the foregrounds and the number of frequency channels and multipole modes available to minimize this variance. Since the variance of the foregrounds is much larger at the reionization scales ($\ell \simeq 10$), parametric fitting was preferred to reconstruct CMB B-modes at low multipoles $\ell < 50$ (reionization peak), while blind methods were used to reconstruct the signal at large multipoles $\ell \geq 50$ (recombination peak).

2.3 Results

The left panel of Fig. 1 shows the reconstruction of the primordial CMB B-mode after foreground cleaning with COMMANDER and SMICA for a fiducial tensor-to-scalar ratio of $r = 5 \times 10^{-3}$, in the absence of lensing. The broad frequency range of *CORE* allows us to recover the primordial B-mode signal at both reionization and recombination peaks, and to measure the posterior distribution of $r = 5 \times 10^{-3}$ without bias at 12σ significance (right panel of Fig. 1) after foreground cleaning. In the presence of lensing contamination, a shortcut was adopted to perform

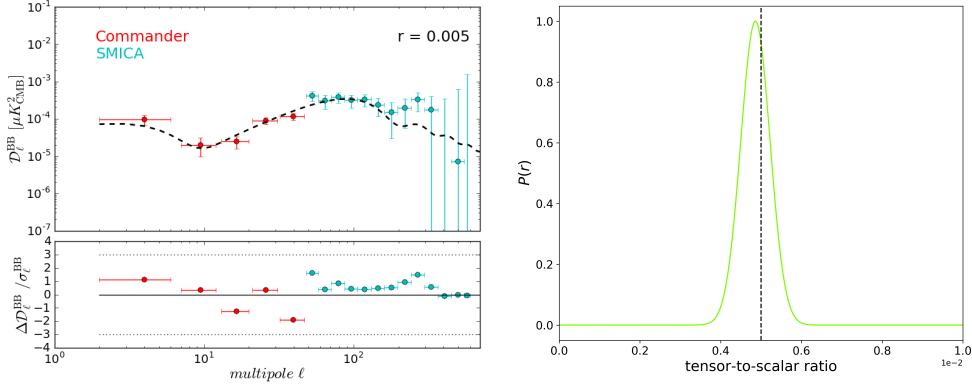


Figure 1 – Primordial B-mode reconstruction at $r = 5 \times 10^{-3}$ (left) and estimate of r (right) for *CORE*.

delensing. Instead of correcting for the lensing variance in the foreground-cleaned CMB B-mode map, as real delensing approaches would do, we left 40% of the lensing B-mode power in the CMB map realization of the simulation, then performed foreground cleaning on the modified simulation. This is equivalent to performing foreground cleaning and 60% delensing, which is the delensing capability quoted by *CORE*¹³. In the presence of lensing, $r = 5 \times 10^{-3}$ is detected at 4σ significance after foreground cleaning and 60% delensing⁶, putting *CORE* in an excellent position to constrain the energy scale of inflation for the Starobinsky’s R^2 inflation model¹.

For a tensor-to-scalar ratio as low as $r = 10^{-3}$, the residual foreground contamination in the CMB B-mode power spectrum after component separation is significant at all angular scales for all the methods⁶, resulting in a 3σ bias on the measurement of $r = 10^{-3}$ by *CORE*. The bias is attributed to the available frequency range 60-600 GHz of *CORE*, for which the minimized variance of the foregrounds achieved by blind methods (NILC and SMICA) still exceeds $r = 10^{-3}$ in power while being lower than $r = 5 \times 10^{-3}$. For parametric methods (COMMANDER), the absence of frequencies below 60 GHz prevent the synchrotron spectral index, β_s , to be constrained at the level of precision required for $r = 10^{-3}$: while the recovered distribution of β_s over the sky has same mean and standard deviation than the actual distribution, it is more Gaussian-distributed, which results in a 2% mismatch on β_s . This error on β_s is large enough to cause an excess B-mode power at a level of $r \approx 2.5 \times 10^{-3}$ when extrapolating synchrotron B-modes to CMB frequencies⁶. Subpercent precision on foreground spectral indices is thus required to measure $r = 10^{-3}$ without bias, which can be achieved with broader frequency ranges (Sect. 3).

3 Concluding remarks: subtle issues for B-mode component separation

On the importance of a broad frequency range. The CMB satellite concept *PICO*⁵ benefits from a broader frequency range (21-800 GHz) than *CORE*. The reconstruction of the CMB B-mode power spectrum at $r = 10^{-3}$ with *PICO* is shown in the left panel of Fig. 2, for the same sky simulation. Due to a larger frequency range of 21-800 GHz, *PICO* allows COMMANDER to control the foreground contamination at the desired accuracy to measure $r = 10^{-3}$ with 2.5σ significance, without any bias, from low multipoles $2 \leq \ell \leq 50$. Conversely, narrowing the baseline frequency range of *PICO* to 43-462 GHz (right panel of Fig. 2) introduces a bias at large angular scales on the recovered B-mode power spectrum because of residual dust contamination. In the absence of high frequencies $\gtrsim 400$ GHz, the dust MBB temperature is constrained with lower accuracy (left-corner stamp in the right panel of Fig. 2), which results in spectral degeneracies in the fit and translates into a bias on the reconstructed CMB B-mode at $r = 10^{-3}$.

Foreground mismodelling. Due to the very large dynamic range between foregrounds and CMB B-mode fluctuations, component separation for polarization is much more sensitive to foreground modelling uncertainties than for temperature. Mismodelling two MBB dust components as a single MBB dust component in the COMMANDER fit was shown to bias $r = 5 \times 10^{-2}$

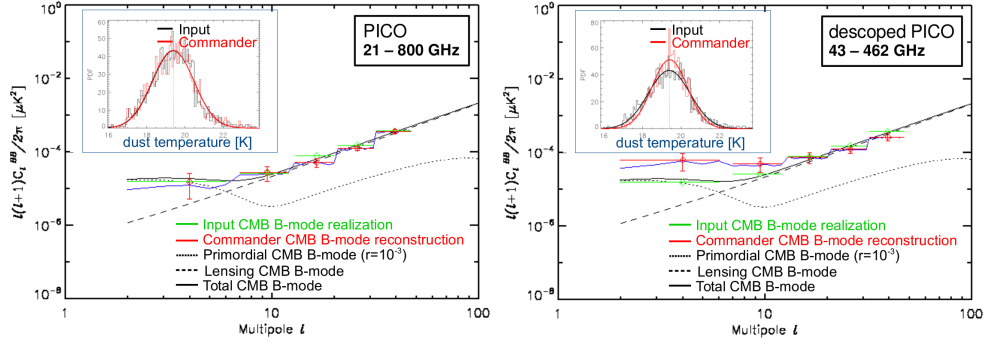


Figure 2 – CMB B-mode reconstruction for *PICO* 21-800 GHz (left) versus *descoped PICO* 43-462 GHz (right).

by more than 3σ for any CMB satellite concept¹⁴. Most important, CMB experiments with narrower frequency ranges show no chi-square evidence for incorrect dust modelling¹⁴, the fit of the overall sky emission being still accurate in narrow frequency ranges while it suffers from spectral degeneracies. Frequencies below 60 GHz and above 400 GHz are thus critical for CMB B-mode experiments to get chi-square evidence for incorrect foreground modelling and false detections of r . It could be argued that increasing the frequency range of observations will introduce additional foregrounds. However, Galactic foregrounds are not fully decorrelated across frequencies, so that the increase in foreground complexity (extra degrees of freedom) should be more than compensated by the increase of information (extra frequencies) for component separation.

Spectral averaging effects. Foreground spectral indices vary in the sky from line-of-sight to line-of-sight, but sky map observations are pixelized and do not have infinite resolution, so that different spectral indices are averaged within pixels or beams¹⁵. The averaging of power-laws with different spectral indices in a pixel is no longer a power-law, instead it introduces spurious curvatures in the effective emission law across frequencies⁶. Say otherwise, the effective emission laws of the foregrounds on the pixelized maps may differ from the real emission laws in the sky. Averaging effects are critical for parametric fitting methods in the context of B-modes. Ignoring in the parametric fit a spurious dust curvature of 0.05 caused by averaging effects results in a bias of $\Delta r \gtrsim 10^{-3}$ on the tensor-to-scalar ratio⁶. To tackle this issue, moment-expansion approaches¹⁵, rather than astrophysical model fitting, might provide an interesting avenue.

Acknowledgments

The author acknowledges funding from the ERC Consolidator Grant *CMBSPEC* (No. 725456).

References

1. Starobinsky A. A., Sov. Astron. Lett. **9**, 302 (1983)
2. Matsumura T. *et al*, Journal of Low Temperature Physics **184**, 824 (2016)
3. Delabrouille J. *et al*, JCAP **4**, 014 (2018)
4. Kogut A. *et al*, JCAP **7**, 025 (2011)
5. https://zzz.physics.umn.edu/ipsig/_media/aasoral2018_v6.pdf
6. Remazeilles M. *et al*, JCAP **4**, 023 (2018)
7. Delabrouille J. *et al*, A&A **553**, A96 (2013)
8. Planck Collaboration *et al*, A&A **596**, A109 (2016)
9. Miville-Deschênes *et al*, A&A **490**, 1093 (2008)
10. Ali-Haïmoud *et al*, MNRAS **395**, 1055 (2009)
11. Planck Collaboration *et al*, A&A **594**, A10 (2016)
12. Stompor R. *et al*, Phys. Rev. D **94**, 083526 (2016)
13. Challinor A. *et al*, JCAP **4**, 018 (2018)
14. Remazeilles M. *et al*, MNRAS **458**, 2032 (2016)
15. Chluba J. *et al*, MNRAS **472**, 1195 (2017)